

UC Santa Barbara

UC Santa Barbara Previously Published Works

Title

Exploring how molluscan purple has survived throughout the Ages: The excited state dynamics of 6,6'-dibromoindigotin

Permalink

<https://escholarship.org/uc/item/9st8v6k8>

Authors

Cohen, Trevor

Didziulis, Julia

Smith, Charles

et al.

Publication Date

2024-05-01

DOI

10.1016/j.chemphys.2024.112271

Peer reviewed

Exploring how Molluscan Purple has Survived throughout the Ages: The Excited State Dynamics of 6,6'-Dibromoindigotin

Trevor Cohen^a, Julia Didziulis^a, Charles Smith^a, Michal F. Rode^b, Andrzej L. Sobolewski^b, Ioannis Karapanagiotis^c, and Mattanjah S. de Vries^a

^a Department of Chemistry and Biochemistry, University of California Santa Barbara, CA 93106-9510, USA. ^b Institute of Physics, Polish Academy of Sciences, Warsaw, Poland. ^c Department of Chemistry, Aristotle University of Thessaloniki, Greece.

Abstract

The color purple has long been used as a symbol of royalty and power in art, fashion, and architecture. This correlation with aristocracy can be traced back to the use of molluscan purple, a rich purple dye that is still presently more expensive than gold, by royalty as early as the 18th century BCE. While the molluscan purple dye is composed of a mixture of various proteins, its color is derived from indigotin, indirubin and their brominated derivatives, including the molecule, 6,6'-dibromoindigotin, an analogue of the indigotin dye which is also widely used in various modern industries. Both dyes can exhibit high stability, in particular against photodamage from UV and Visible radiation. In this study, we present the gas phase absorption spectrum and excited-state lifetimes of 6,6'-dibromoindigotin combined with static calculations of the excited and ground-state potential energy surfaces. The lifetime measurements reveal that molluscan purple has nearly the same relaxation rate as indigotin providing new insights in the possible relaxation mechanisms of the indigotin family of dye molecules.

1. Introduction

The use of molluscan purple in wall paintings and textiles dating back up to the 18th century BCE, has been revealed through archaeometric investigations which reported the chemical identification of the purple pigment in archaeological fragments.[1, 2] Moreover, these findings are supported by heaps of molluscan shells found in archaeological sites of the Mediterranean (e.g. in Coppa Nevigata, Aegean islands, Phoenicia, etc).[1-3] The name molluscus purple comes from snails which in huge quantity were used to dye fabrics in ancient times. 1 gram of this dye is obtained from the secretion of 10,000 of these large sea snails. Molluscan (or shellfish) purple is known also as Tyrian purple, because of its significant role in the history of the maritime Phoenician trade, or royal/imperial purple, since the expensive purple-dyed textiles were status symbols. It should be stressed, however, that the message derived from the terms *royal* or *imperial* purple might be misleading, because in certain historical periods and geographical areas molluscan purple was not reserved exclusively for members of the royal family. For example, purple fragments of (i) wall paintings in the Raos-Thera site (Late Bronze Age), (ii) a textile in Lakkoma (Hellenistic period) and (iii) a textile in Thessaloniki (Roman period) are not linked to members of royal families, but rather to prominent citizens and high-ranking officials.[1, 2, 4, 5]

The cultural relevance and trade of molluscan purple can be well tracked throughout history because the dye is well preserved due to the structural stability of the primary chromophores, which provide its color on a multitude of art media such as pottery, paintings, and textiles.[6, 7] The chemical identification of molluscan purple is achieved by the detection of brominated-indigotins, such as the 6,6'-dibromoindigotin (Figure 1) which was reported as a coloring constituent of *Murex brandaris* extracts at the beginning of the 20th century.[8, 9] Apart from the brominated-indigotins, the color of molluscan purple, is also affected by the brominated-indirubins which, however, are usually reported in small amounts.[4]

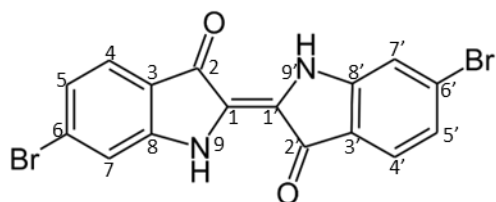


Figure 1: The chemical structure of 6,6'-dibromoindigotin (molluscan purple) in the trans-diketo tautomeric form.

Both Indigo and Molluscan Purple in their diketo form are structurally related to many natural dyes, such as e.g. dipyrrolonaphthyridinediones, which are cross-conjugated donor-acceptor chromophores.[10] One of the most prominent environmental pressures on pigments used in art is their exposure to the sun's rays.[11] Notably, a material cannot be colored without absorbing visible light. The photostability of a molecule is often inversely related to its excited-state lifetime, which is a measure of how quickly a molecule can return to the ground state upon photoexcitation.[12] While 6,6'-dibromoindigotin has scarcely been studied due to its cost, either to synthesize or harvest, the excited-state dynamics of indigotin is well established. Calculations of the excited-state potential energy surface revealed that the molecule undergoes an intramolecular proton and hydrogen transfer tautomerizing from the diketo to the keto-enol conformation.[13, 14] The potential energy surface and the barrier to transfer was found to be primarily dependent on the N-H coordinate donor and O acceptor distances.[8] Solution phase and matrix isolation studies sought to observe these calculated proton transfer processes on ultrafast timescales through fluorescence, transient absorption, and photoisomerization, but found no evidence of the transfer.[15-20] Other studies tried to monitor the predicted proton transfer by measuring the dynamics of related forms of indigotin such as the reduced leuco-indigotin and the dianion indigotin carmine.[21-25] Those studies could not measure this relaxation channel but did find an ultrafast decay to the ground state.

Haggmark et al. measured the structure, excitation spectra, and excited-state lifetimes of indigotin (I_0) in the gas phase to investigate the proposed excited-state intramolecular proton and hydrogen transfer (PT and HT respectively) in a solvent-free environment.[26] In that work we found that unlike in common excited state intramolecular proton (ESIPT) systems, indigotin also exhibits hydrogen transfer as part of its photochemistry. Experimentally we observed two

deactivation processes, a faster and a slower one. Calculations predicted two pathways as well, involving PT and HT, respectively, in the excited state and the opposite character (HT and PT) in the ground state trajectories. The excited-state potential-energy surfaces show trajectories with sequential double proton or hydrogen transfer.[27] There is a narrow spectral range (up to about 1000 cm^{-1} above the origin) in which the partitioning among the two pathways depends strongly on vibrational modes. Above 1000 cm^{-1} the excited-state lifetime shortens considerably, providing a mechanism for indigotin's stability against radiative damage.

The effects of halogenic substitution on proton transfer have been studied extensively due to its diverse applications in electronics and solar cells, and its presence in biological systems.[28] Typically, the addition of a strong electron-accepting group to a molecule draws electron density away from the proton increasing the rate of transfer. Studies on structures similar to the diketo indigotin tautomer found that fluorination also stabilizes the compound with a strong dependence on the position of the substitution, and results in changes in the excited-state lifetime.[29]

Here we present the absorption and excited-state dynamics of 6,6'-dibromoindigotin in the gas phase using resonance enhanced multi-photon ionization and pump-probe spectroscopy along with calculations of the excited-state potential energy landscape for comparison with its non-brominated form. Bromination of indigotin resulted in a blue-shift of the absorption spectrum near the origin transition. However, the excited-state dynamics appears to be very similar to that of I_0 . Like indigotin, molluscan purple exhibits two distinct decay processes on the order of 1 and 20 ns respectively. Computations of excited state profiles are also very similar to those for I_0 with only a $\sim 0.007\text{ eV}$ difference in the calculated second proton transfer barrier height. Based on these results, we speculate upon the complete relaxation mechanism of the indigotin family which we find to be a useful model for the more complex and historically relevant molluscan purple.

2.Methods

2.1. Experimental

We have previously described the REMPI technique in detail and will only briefly describe the specifics of our experiment here.[30] Molluscan purple was synthesized according to a methodology previously described.[4] Solid molluscan purple was deposited onto a graphite bar and placed into the experiment chamber under high vacuum (2×10^{-6} torr). The sample is laser desorbed with a focused 1064 nm pulse from a Continuum Minilite I laser (10 Hz, 5 ns pulse width) which vaporizes the sample with minimal fragmentation. To continually refresh the material for desorption, the sample substrate is translated with a stepping motor orthogonally to the laser. The vaporized material is entrained in argon pulsed into the chamber (10 Hz, 8 Bar backing pressure) cooling the material to $\sim 15\text{ K}$ and directing the material through a skimmer into a detection region for further analysis.

To measure the excitation spectra and excited-state lifetimes of molluscan purple, REMPI and pump probe spectroscopy are employed. The laser pulses used for both spectroscopic techniques are generated from the third harmonic of an EKSP LA PL2251 Nd:YAG laser (30 ps pulse width, 1064 nm fundamental), pumping a PG-401 tunable optical parametric generator capable of

producing wavelengths from UV to NIR with 6.5 cm^{-1} resolution and approximately $600\ \mu\text{J}$ pulses. For REMPI, the wavelength of a tunable visible light pulse is scanned and resonant absorption promotes the molecule to the excited state. A second pulse, produced from 5th harmonic generation of the fundamental from the same pump laser source, provides enough energy to ionize the molecule only if successfully excited. The resulting ions are detected in a time-of-flight mass spectrometer, thus providing simultaneous mass and absorption monitoring of 6,6'-dibromoindigotin. To perform pump-probe spectroscopy, the excitation laser is parked on a vibronic transition. A mechanical delay stage (Thorlabs, 300mm delay) in the 5th harmonic laser pulse pathway provides up to a 2 ns delay with approximately 6 ps resolution. The relative ion count is measured as a function of delay. A separate ionization pulse generated from the 5th harmonic of a Quantel DCR-11 Nd:YAG laser (5ns pulse width, 10 Hz, 8mJ/pulse) electronically delayed by a Stanford Instruments DG-645 delay generator measures the pump probe spectra with nanosecond delay. For both ns and ps pump probe experiments, resultant decay spectra are convolved and fitted to a monoexponential decay in a Mathematica script.[31]

2.2. Computational

The methodology used for Molluscan Purple is analogous to the one used for the indigo and deuterated indigo molecules.[27] The equilibrium geometry of the diketo form (Fig. 1) – the most stable planar minimum of the Molluscan Purple molecule – in its closed-shell ground electronic state (S_0), was determined with the MP2 method [32] with C_s symmetry constraint. The MP2 energy of the diketo form in the S_0 -state is the reference value for all other ground-state and excited-state structures. The excited-state (S_1) equilibrium geometries were determined with the second-order algebraic diagrammatic construction ADC(2) method[33-36]. For the molluscan purple molecule, the correlation-consistent valence double-zeta basis set with polarization functions on all atoms (cc-pVDZ)[37] was used in these calculations as well as in the calculations of potential energy profiles as it was done for the indigo molecule.[27] The triple-zeta (cc-pVTZ) basis set[37] was used only for bromine since it is a fourth row element.

To study the process of the transfer of the two active protons in the excited state of the diketo form, the relaxed potential energy profiles were calculated: first, along the first NH coordinate, R_1 (N1-H), and subsequently along the second NH coordinate, R_2 (N2-H). For each fixed value of a given NH coordinate the remaining internal nuclear coordinates were optimized.

To simulate the UV absorption spectra, the approximate coupled cluster singles and doubles method was used, CC2[38, 39] in conjunction with the cc-pVTZ basis set. Next, the CC2 results were compared to the ADC(2) results. The cc-pVTZ basis set was used also for optimization of the ground and excited state forms of molluscan purple and indigotin, for comparison and benchmarking. All calculations were performed using the TURBOMOLE program package.[40]

3.Results

3.1. Experimental Results

Figures 2(a) and (b) show the R2PI spectra of molluscan purple with 30 picosecond and 6 nanosecond ionization laser pulses respectively. Both spectra use the same excitation laser, but a different ionization laser depending on the timescale required. The origin transition was found to

be at 18416 cm^{-1} (2.28 eV), representing a 267 cm^{-1} (0.03 eV) blue shift relative to indigotin. This slight blue-shift is well reproduced by calculations of the S_0 - S_1 transition to be 2.30 eV, for molluscan purple and 2.28 eV for indigotin ($0.018\text{ eV} = 145\text{ cm}^{-1}$ see benchmarking calculated spectra in the supporting information). Absorption spectra in a solution of DMF were reported with a similar although smaller shift.²⁰ Both spectra were plotted as a function of excess energy with respect to the origin transition. We distinguish two regions of excitation, one, denoted as A, spanning from the origin to approximately 500 cm^{-1} excess energy and the other, denoted as B, at higher excess energy. Region A shows peaks with both picosecond and nanosecond ionization and region B only shows peaks with picosecond ionization. The longer pulse width laser is less efficient at ionizing excited states with sub-nanosecond lifetimes.

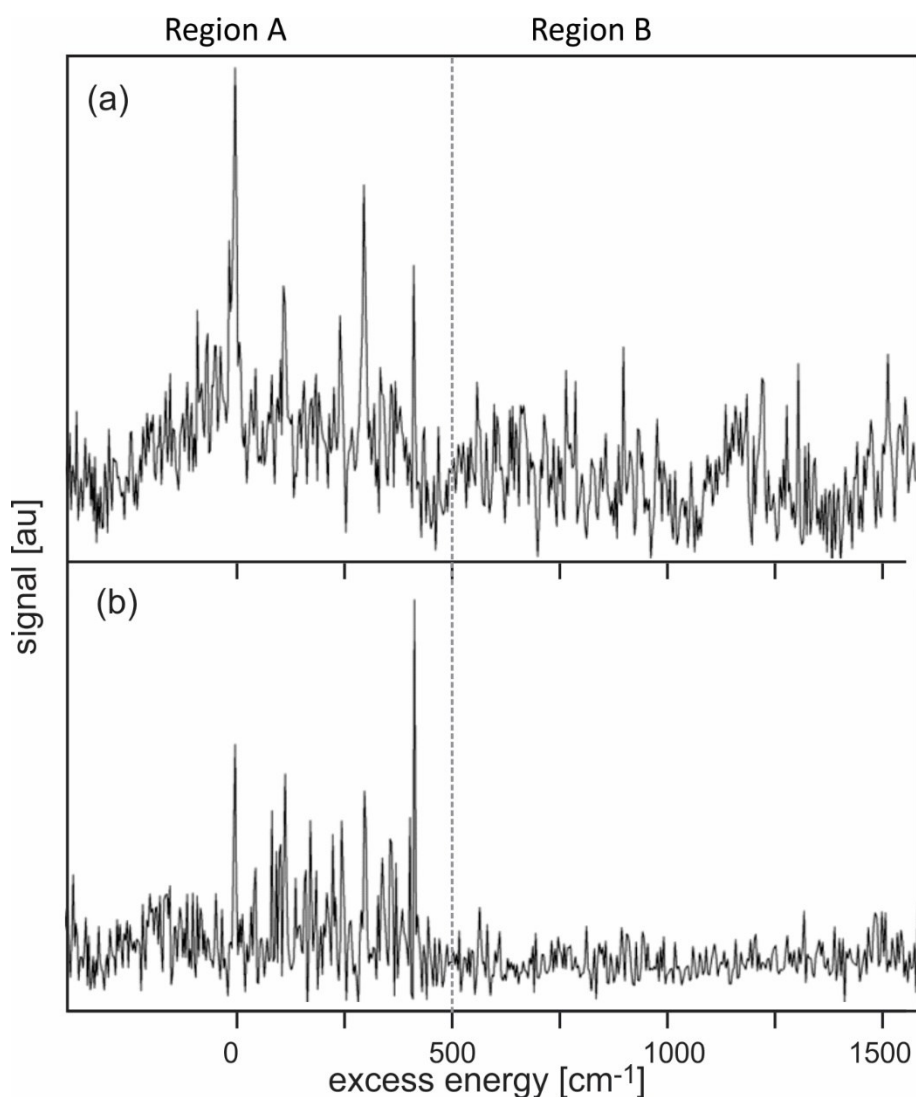


Figure 2: R2PI spectra of molluscan purple with picosecond (a) and nanosecond (b) ionization. The spectra were plotted in excess energy with respect to the origin. For both spectra, region A and B are highlighted in green and red respectively.

S_n	Molluscan Purple		Indigotin	
	ΔE^{VE}	$f(S_0 \rightarrow S_n)$	ΔE^{VE}	$f(S_0 \rightarrow S_n)$
S_0	0.0		0.0	
$S_1(\pi\pi^*)$	2.3002	0.3964	2.282	0.3535
$S_2(n\pi^*)$	3.00	0.0000	3.00	0.0000
$S_3(\pi\pi^*)$	3.14	0.0000	3.13	0.0000
$S_4(n\pi^*)$	3.45	0.0000	3.46	0.0000
$S_5(\pi\pi^*)$	3.70	0.0000	3.79	0.0000
$S_6(\pi\pi^*)$	4.10	0.6135	4.41	0.4066
$S_7(\pi\pi^*)$	4.40	0.5218	4.45	0.2011
$S_8(\pi\pi^*)$	4.42	0.0000	4.60	0.0000
$S_9(n\pi^*)$	5.13	0.0002	5.23	0.0000

Table 1: Calculated UV absorption spectra of molluscan purple vs. indigotin. Vertical excitation energy (ΔE^{VE} , in eV) and oscillator strength, f , of the $S_0 \rightarrow S_n$ transition to the lowest $\pi\pi^*$ and $n\pi^*$ excited singlet states of both molecules calculated with the CC2/cc-pVTZ method at the ground-state diketo geometry optimized at the MP2/cc-pVTZ (cc-pVTZ@Br) theory level.

We performed pump-probe spectroscopy with picosecond and nanosecond delays (using picosecond and nanosecond ionization pulses, respectively) to measure the excited-state lifetimes of molluscan purple. In our previous study of non-substituted indigotin (I_0), we found two decays for excitation energies in region A on the order of 1 and 20 ns.[24, 25] Only the diketo tautomer was observed in the indigotin experiment, we assume this remains true for 6,6'-dibromoindigotin. Figure 3 shows the pump-probe spectrum at the origin transition with picosecond ionization pulses, which can be fit monoexponentially to an approximate 2.5 ns lifetime. This lifetime is about 1.5 ns longer than for the origin transition of I_0 but within the same order of magnitude as the lifetimes measured in region A of indigotin. Figure 4 shows a pump-probe spectrum of the origin transition with nanosecond ionization pulses, fit to a 20 ns excited-state lifetime. As discussed below, these lifetimes are of the same order as those for I_0 and the differences between them are within the precision of the fitting algorithm (100 ps for the ps pump probe, 3 ns for the ns pump probe). Measurement of a higher energy transition, found in Figure S1, produced analogous lifetimes on this time scale.

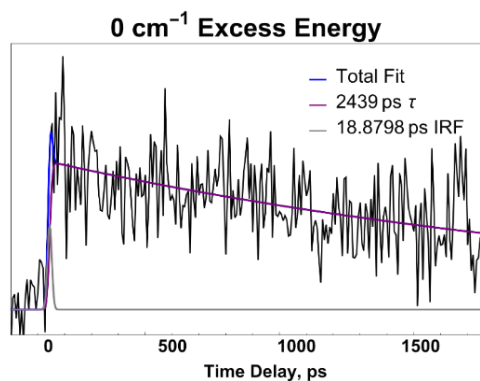


Figure 3: Pump probe of molluscan purple taken with a picosecond delay at the origin transition.

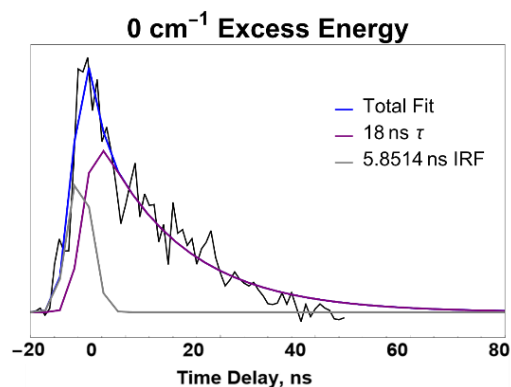


Figure 4: Pump probe of the origin transition with nanosecond delay.

3.2. Computational Results

Bromination at the 6 and 6' sites of indigotin withdraws the electron density from indigotin towards the halogens potentially influencing the shape of the previously calculated sequential double-proton transfer energy landscape. To confirm this, we modelled the adiabatic excited-state potential-energy (PE) profile (filled in squares and triangles) as well as the vertical PE profile in the ground state (empty squares and triangles) at the ADC(2) and MP2 level respectively. Figure 5 displays the calculated lowest energy 1-D trace of one trajectory of the excited-state and ground-state PE profile as a function of these two coordinates. Each point of the ground-state PE profile for the given coordinate value shown in Fig. 3 (empty squares and triangles) is calculated at the geometry optimized in the excited-state (full squares and triangles). The fluorescence energy is calculated as the difference between the energies of the S_1 and S_0 states.

The overall excited-state energy landscape of the molluscan purple molecule is strikingly like indigotin. 6,6'-dibromoindigotin retains the same C_s symmetry as indigotin making the order of the proton transfer indistinguishable. Since only the trans-diketo tautomer was present in the cold jet of the experiment, this is the tautomeric form we assumed both in the ground state and in the excited state in the Franck-Condon region. It was found in all indigotin analogues that the enol-enol conformer formed from isomerization via double proton transfer is located at a local minimum on the excited-state energy landscape (right half of figure 5). Additionally, the barrier

for concerted double-proton transfer to this conformation is significantly higher than the competing sequential process and is deemed not probable to occur.[27] Calculations were first performed by freezing the first transfer coordinate, denoted N_1H , at various positions and optimizing the remaining coordinates to minimize the energy of the S_1 state. These measurements are found in the left half of Figure 5. The resulting computations suggest a small barrier (0.11 eV high, the same as for indigotin) to transfer as the N_1H coordinate stretched to about 1.18 Å. Beyond the barrier, two trajectories that were nearly isoenergetic in the Franck-Condon region, X (red triangles) and Y (blue squares), begin to deviate slightly in energy and form two distinct keto-enol photoproducts of the first transfer. The relative adiabatic energies (see S_1^a in Table 3) of the X and Y products are 1.893 and 1.869 eV, both lower in energy than the corresponding S_1^a of I_0 products (1.899 and 1.875 eV, respectively). These two states differ in the amount of electric charge carried during the transfer, and we denote them as the first proton and hydrogen transfers respectively. Additionally, the center C-C bond length in 6,6'-dibromoindigotin is significantly longer in the X trajectory (1.453 Å) than the Y (1.383 Å), as seen in Table 2. The C-C bond lengths along both X and Y trajectories are the same as the corresponding traces in I_0 . As the coordinate is stretched further beyond the barrier, the two states remain close in energy.

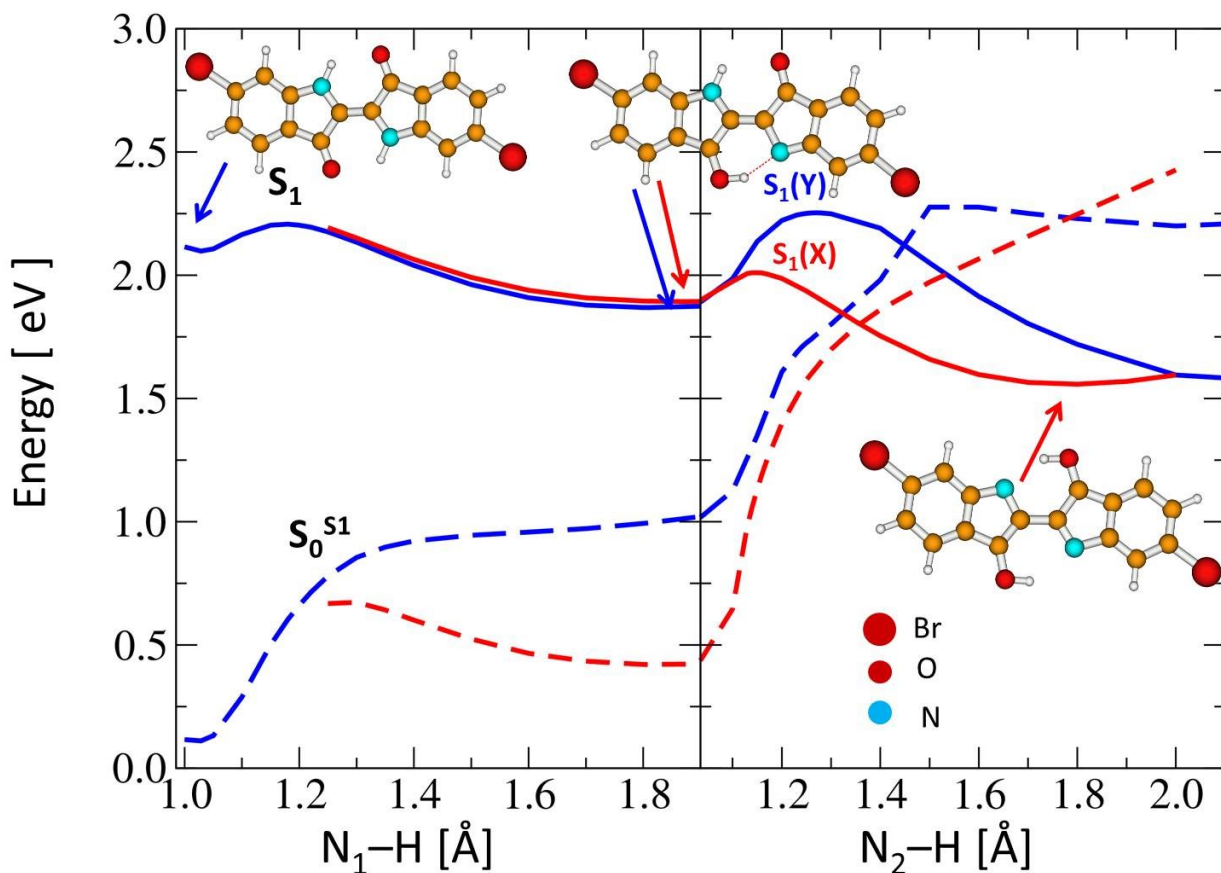


Figure 5: Two minimum energy profiles of Molluscan Purple (calculated with the ADC(2)/cc-pVDZ method) plotted as a function of N_1-H distance (left side) describing first ESIPT overcoming the barrier towards keto-enol form, and N_2-H distance (right side) describing second ESIPT overcoming second barrier towards enol-enol tautomer through

conical intersection region. Solid lines denote minimum-energy profiles of the S_1 state which points represent geometries optimized in the excited state. Dashed lines (S_0^{S1}) denote energy profiles of the S_0 state computed at the optimized geometries of the S_1 state. Red solid lines describe excited-state proton transfer, $S_1(\mathbf{X})$, blue solid lines – excited state hydrogen transfer $S_1(\mathbf{Y})$. See text for details.

Molluscan Purple, ground state (S_0)				Indigotin, ground state (S_0)			
	diketo	X, enol-keto	Y, enol-keto		diketo	X, enol-keto	Y, enol-keto
S_0 [eV]	0.00	-	0.142	S_0 [eV]	0.00	-	-
μ_g [D]	0.00	-	1.38	μ_g [D]	0.00	-	-
C_1 - C_2 [Å]	1.364	-	1.406	C_1 - C_2 [Å]	1.365	-	-
Molluscan Purple, singlet excited state (S_1)				Indigotin, singlet excited state (S_1)			
	diketo	X	Y		diketo	X	Y
S_1^a [eV]	2050	1.850	1.819	S_1^a [eV]	2.031	1.851	1.824
E_{fl} [eV]	1.941	1.404	0.810	E_{fl} [eV]	1.922	1.388	0.785
$f(S_1 \rightarrow S_0)$	0.3057	0.213	0.0972	$f(S_1 \rightarrow S_0)$	0.273	0.1783	0.0838
μ_e [D]	0.0 D	7.03	3.48	μ_e [D]	0.00	6.89	3.64
C_1 - C_2 [Å]	1.385	1.441	1.370	C_1 - C_2 [Å]	1.385	1.443	1.371
τ_r [ns]	10	5.4	2.3	τ_r [ns]	10.8	6.2	2.4

Table 2: A comparison of the calculated ground (S_0) and excited-state (S_1) adiabatic energies, fluorescence energy (E_{fl}), dipole moment (μ_g , μ_e), oscillator strength of the $S_1 \rightarrow S_0$ transition (f), and C_1 - C_2 bond length of the diketo and enol-keto tautomers between molluscan purple and indigotin calculated using the MP2/cc-pVTZ method for S_0 and ADC(2)/cc-pVTZ for the S_1 state. The calculated fluorescence lifetimes (τ_r , in blue) are shortened in all calculated conformations of molluscan purple. E_{fl} is calculated at the excited-state minimum geometry as the energy gap between the S_1 and S_0 state. The C_2 - C_2 distance is given to emphasize the different – single or double character of the bond in the ground or excited state \mathbf{X} or \mathbf{Y} enol-keto structure.

The right half of Figure 5 similarly freezes the second transfer coordinate, N_2H , at various distances and plots the energies of the optimized structures for both the \mathbf{X} and \mathbf{Y} paths. Stretching this coordinate to about 1.3 angstroms in both conformers results in the formation of a second barrier to transfer. However, unlike the barrier in the N_1H coordinate, the barriers in the \mathbf{X} and \mathbf{Y} trajectories differ greatly, with heights of 0.117 eV and 0.382 eV, respectively. Those two barriers are just slightly lower than the corresponding barriers for indigotin, 0.124 and 0.401 eV.[27] Beyond these barriers both trajectories form conical intersections with the ground-state trace,

leading to a ground-state intramolecular back transfer which eventually reforms the trans-diketo tautomer.

Bromine substitution at the 6 and 6' positions results in a small shift of the calculated potential energy profile compared to indigotin slightly altering the dynamics of the transfer process. The first transfer barrier had no change in height compared to indigotin (0.11 eV). However, both the X and Y barriers to second transfer showed slight decreases in height relative to the indigotin barrier, by 0.007 and 0.019 eV respectively. Additionally, the gap between the peaks of the two barriers increased by 0.012 eV from 0.253 eV in indigotin to 0.265 eV in molluscan purple, suggesting an increased preference to proceed along the X pathway. The fluorescence lifetimes (see τ_r in Table 2) of the keto-keto tautomer and the X (PT) and Y (HT) products were also estimated to be 10, 5.4, and 2.3 ns respectively, according to the formula $\tau_r = 4/3 \pi c \lambda^3 f$, where c is the speed of light [m/s], λ and f are fluorescence wavelength [m] and oscillator strength of $S_1 \rightarrow S_0$ transition, calculated with the ADC(2)/cc-pVTZ method (see Table 2).

4. Discussion

4.1 REMPI

The signal to noise in the REMPI spectra is quite poor because of the small amount of precious material we had available, which limited the amount of signal averaging we could perform. Therefore, a detailed vibronic analysis is not possible. Nevertheless, two observations stand out. First, the origin is blue-shifted relative to that of I_0 by 267 cm^{-1} , matching the 0.02 eV increase in excitation energy calculated to reach the S_1 for Molluscan Purple found in Table 1. Secondly, the ns ionization spectrum exhibits a sharp cut-off at 500 cm^{-1} compared to 1000 cm^{-1} in the case of I_0 . This cut-off indicates the energy beyond which the excited state lifetime becomes too short to allow ionization by the 6 ns pulses of the ionization laser.

4.2 Excited-State Dynamics

To completely model the excited-state dynamics, dynamics simulations are required which is beyond the scope of this experimental study. However, we will speculate on the possible processes the indigotin family utilizes to remain photostable and discuss how the dibromo analogue of indigotin provides new insight towards identifying the mechanism.

Our earlier studies of unsubstituted indigotin showed that upon excitation in the Frank Condon region, indigotin relaxes on two distinct time scales on the order of 1 and 20 ns, respectively.[26] Accompanying computational calculations of the excited-state potential energy landscape as a function of the N_1 -H coordinate, responsible for excited-state intramolecular proton and hydrogen transfer indicated that upon overcoming a 0.11 eV barrier to transfer, two distinct trajectories form nearly isoenergetic X and Y keto-enol isomers. Along the second N_2 -H coordinate the two trajectories deviate in energy, both forming a second barrier to transfer. The barrier on the Y trajectory is approximately 0.3 eV higher than that for X, and we tentatively assigned the

faster lifetime to X and slower to Y. We selectively substituted the hydrogens that take part in excited-state intramolecular proton and hydrogen transfer with deuterium atoms and found that only the faster relaxation process exhibited a kinetic isotope effect (KIE).[27] We concluded that the faster mechanism involves tunneling through at least one of the S_1 -state potential energy barriers. These results suggest that the longer lifetime involves a process not affected by deuteration such as fluorescence or relaxation along an entirely different reaction coordinate.

The pump probe spectra of dibromo indigotin on the nanosecond and picosecond timescales show no change in lifetime compared to indigotin. Furthermore, the calculated S_1 -state energy landscape shows minimal change to the trajectories pre- and post-hydrogen and proton transfer, suggesting that this indigotin analogue uses the same mechanisms to relax as I_0 . While the two measured mechanisms cannot be definitively assigned, we discuss below how the bromination affects each of the proposed mechanisms.

4.2.1 The Fast Process

Stasyuk et al. reviewed the effect of substitution with strong electron-withdrawing groups on excited-state proton and hydrogen transfer.[28] Fores et al. identified a few key characteristics that impact the transfer processes. Halogenic substitution on the donor side stabilizes the pre-proton transfer tautomer in the ground and excited state while acceptor side substitution stabilizes the post-transfer product.[29] However, while the proton transfer product is slightly lower in energy when substituted on the acceptor side, the barrier to transfer increases and the converse effect occurs for donor side substitution. Yang et al. found that placement of a fluorine atom para to the hydrogen transfer donor favors the forward transfer strongly, while the back transfer rates in the ground state greatly diminish and the overall rate decreases.[41] Meta substitution increases the rates of both, illuminating the importance of the distance of the electrophilic group to the transfer site. In general, the heights of the ESIPT barriers are very sensitive to the position of the substituents and also dependent on the number of substituents.[42] It is not always predictable, however, how the placement of electron withdrawing groups affect these processes.

For 6,6'-dibromoindigotin, the excited-state transfer sites are likely destabilizing the keto tautomer in the excited and ground state. The exoenergeticity of the first proton transfer increases from -0.188 eV (indigotin, X-path, S_1^a in Table. 3) down to -0.205 eV (molluscan) while the height of energy barrier remains the same. Additionally, we found a slight decrease in the second barrier height on the excited-state potential energy profile compared to I_0 which could increase the tunneling rate and lower the lifetime. However, we observed no significant change in the excited-state lifetime of the faster process. Measurements of the kinetic isotope effect in I_0 point towards a tunneling mechanism, but it is not conclusive which of the two barriers are involved. It is of note that the experimental measurements and calculated potential energy landscape do not account for any possible changes in the rate of the ground state back transfer which others have found to shift with halogen substitution. But like in the excited state, the change in the potential-energy landscape in the ground state does not change significantly. While a faster rate of ESIPT and ESIHT are both predicted from the lower calculated barrier if tunneling is involved as well as from previous studies of donor-side halogenic substitution, we postulate that we did not observe this change in rate in our pump-probe spectra because: (1) the calculated

barrier height change is too small to have a measurable effect on the tunneling rate with the limited resolution afforded by our fitting algorithm, (2) tunneling only occurs through the first barrier, for which the height was unchanged, and (3) the bromine atom is too far away from the donor-acceptor sites to influence the transfer processes. Bromine is also a weak electron acceptor as well as weak electron donor, both in the ground[SE-S₀][43] and in the excited state[SE-S₁],[44] according to calculated sEDA and pEDA parameters, further reducing its influence on the energetic landscape.

Further adiabatic calculations of 7,7' and 4,4' dibromo indigotin, positioning the bromines closer to the nitrogen and oxygen groups on indigotin respectively, exhibit large changes in the exoenergeticity for the keto-keto and keto-enol tautomers and large shifts in the second transfer barrier heights (Table 3). This effect is especially prominent in 4,4'-dibromo indigotin which has the largest differences in adiabatic energy between the X and Y keto-enol products resulting in the most exothermic first transfer process (ΔE^X enthalpy = -0.228 eV). Additionally, the X product in the 4,4' derivative has the largest dipole moment among the indigotin molecules studied here. 4,4' dibromo indigo has the lowest second transfer barrier height which should result in the fastest internal conversion process to the S₀. In contrast, 7,7' dibromo indigotin, which places the bromines closer to the amine group, has the highest second barrier to transfer.

It seems that large electron bromine substituent attracts the two protons (H₁ and H₂) when being close to them in the 7,7'-dibromo molecule, which results in enlarging the N...O and NH...O intramolecular distances in two intramolecular hydrogen bonds and makes the double ESIPT process less effective. In contrast, in the 4,4'-dibromo derivative – bromines repulse oxygen atoms and thus the intramolecular distances become shorter. This results in a more exoenergetic process with lower barriers (see Figs S1 and S2 in the SI). The results show that especially the decrease of the second barrier is accompanied by shortening of the N...O and NH...O intramolecular bonds.

While not conclusive, these findings further support the notion that the bromine atoms in molluscan purple are likely too far to influence the two transfers.

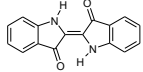
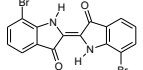
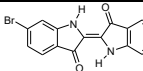
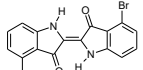
Derivative		S ₁ ^a	S ₁ ^a	S ₁ ^a	ΔE^X	ΔE^Y	1 st barrier	2 nd barrier
		diketo	keto - enol X	Keto - enol Y				
Indigotin, I ₀		2.087	1.899	1.875	-0.188	-0.212	0.109	0.124
7,7'-dibromo-I ₀		2.071	1.877	1.864	-0.195	-0.207	0.114	0.145
6,6'-dibromo-I ₀		2.098	1.893	1.869	-0.205	-0.229	0.109	0.117
4,4'-dibromo-I ₀		2.055	1.827	1.856	-0.228	-0.199	0.114	0.097

Table 3. Comparison of the S_1 -state energetics, in eV, of different dibromo-derivatives of Indigotin. Adiabatic energies (S_1^a) of the diketo, keto-enol-X and keto enol-Y excited-state forms. Enthalpy of the diketo->keto-enol ESIPT process, ΔE^X – for X and ΔE^Y – for Y, respectively, and the S_1 -state energy barriers, in eV, for indigo and its three symmetric dibromo derivatives, calculated with the ADC(2)/cc-pVDZ(cc-pVTZ@Br) method.

The difference between I_0 and dibromoindigotin's calculated fluorescence lifetimes from the X and Y photoproducts is smaller than the resolution of the pump probe experiments. These lifetimes are also close in value to the measured lifetime of the fast process. We conclude that it is likely that the fast process measured for dibromoindigotin utilizes the same tunneling mechanism as I_0 . Upon tunneling through the barrier along the N_1 -H coordinate forming the X and Y photoproduct, both indigotin and molluscan purple can fluoresce from these states. It is also possible that because the second barrier to transfer is low along the X trajectory, the molecule reaches the conical intersection to the ground state. Tunneling through the second barrier along the Y trajectory is unlikely on this timescale because the barrier is too high. After reaching the ground state, a ground state intramolecular hydrogen or proton transfer occurs as calculated for indigotin, reforming the keto-keto tautomer. However, it is not possible to assign which relaxation pathway the indigotins utilize without further dynamics calculations of the excited-state energy landscapes.

4.2.2 The Slower Process

Similarly, the slower process showed no measurable difference in excited-state lifetime compared to the analogous indigotin decay. This decay could be due to several processes. (1) Trapping behind the large barrier in the Y trajectory, followed by adiabatic transfer to the X trajectory. In this case, the small change to the height of the barrier due to bromine substitution would not affect the orders of magnitude slower interconversion to the X trajectory. (2) Fluorescence from the diketo or keto-enol tautomers or (3) a movement to another potential surface through intersystem crossing or internal conversion.

The impact of substitution of heavier atoms and functional groups on lifetime is thoroughly explored in the literature. Theoretical studies have shown that heavy atom substitution increases the rate and quantum yield of intersystem crossing due to increased spin-orbit coupling. This trend has been corroborated experimentally, including for thio- and seleno-substituted indigotin.[45-47] Solution phase studies of molluscan purple and other substituted indigotins in both the diketo and leuco forms showed that in addition to an increase in intersystem crossing quantum yields, the fluorescence yields decreased amongst the available competing mechanisms. Both in molluscan purple and in indigotin, the $^3n\pi^*$ triplet states are lying 0.2 eV above the respective $^1\pi\pi^*$ singlet states and the $^3\pi\pi^*$ triplet states are lying much below so we may speculate that ISC is not the major channel (see Table S2 in the SI).

Like for the fast process, it is unclear which of the possible mechanisms indigotin uses to reach the ground state on this time scale, but we suspect molluscan purple to use the same process as I_0 . We will speculate upon the possible relaxation mechanisms further. An entrapment on the Y

trajectory until interconversion to the X pathway would not exhibit a kinetic isotope effect on this timescale and not be affected by bromination. However, the calculated fluorescence lifetime from the Y state provides a much faster pathway to the ground state and would be in direct competition with this process. Fluorescence from the keto-keto or X trajectory and intersystem crossing occur on the same order of magnitude as the 20 ns lifetime measured. However, similar lifetime studies found that bromination affects the rate of these channels. Future measurements and calculations may also find evidence for an undiscovered trajectory to the ground state that matches the lifetime trends uncovered in these experiments.

5. Conclusion

We present REMPI spectra, pump-probe spectra, and calculated 1-D traces for sequential double proton and hydrogen transfer along the excited and ground-state potential energy surfaces of 6,6'-dibromoindigotin, the major chromophore in the ancient dye known as molluscan purple. Other than a blue-shift in the absorption spectra, molluscan purple shares similar photo-relaxation mechanisms with indigotin: a faster sequential double proton transfer along the X trajectory followed by a back transfer, and a slower interconversion from the Y trajectory to the X profile and followed by the same process. While halogenic substitution in other molecular systems has led to changes in the calculated potential energy surfaces and consequently the rate to transfer, in this case bromination had little effect on the excited-state lifetimes of both decay processes compared to the indigotin molecule. The striking similarities between the measured lifetimes and calculated PES for both indigotin and molluscan purple illustrate the hardness of the two dyes to harmful photodamage as well as the importance of modelling analogous molecules to predict the effects of more complex systems.

Acknowledgements

This work has been supported by the National Science Foundation under CHE-2154787. Calculations were performed at the PL-Grid Infrastructure.

References

- [1] I. Karapanagiotis, A Review on the Archaeological Chemistry of Shellfish Purple, Sustainability-Basel 11 (2019).
- [2] S. Sotiropoulou, I. Karapanagiotis, K.S. Andrikopoulos, T. Marketou, K. Birtacha, M. Marthari, Review and New Evidence on the Molluscan Purple Pigment Used in the Early Late Bronze Age Aegean Wall Paintings, Heritage-Basel 4 (2021) 171-187.
- [3] M.J. Melo, History of Natural Dyes in the Ancient Mediterranean Civilization, in: T. Betschold, A.P. Manian, T. Pham (Eds.), Handbook of Natural Colorants, John Wiley & Sons Ltd.2023.
- [4] I. Karapanagiotis, D. Mantzouris, C. Cooksey, M.S. Mubarak, P. Tsiamyrtzis, An improved HPLC method coupled to PCA for the identification of Tyrian purple in archaeological and historical samples, Microchemical Journal 110 (2013) 70-80.
- [5] I. Karapanagiotis, S. Sotiropoulou, S. Vasileiadou, E. Karagiannidou, D. Mantzouris, P. Tsiamyrtzis, Shellfish Purple and Gold Threads from a Late Antique Tomb Excavated in Thessaloniki, Arachne 5 (2018) 64-77.
- [6] J.C. Splitstoser, T.D. Dillehay, J. Wouters, A. Claro, Early pre-Hispanic use of indigo blue in Peru, Sci Adv 2 (2016).
- [7] R.J.H. Clark, C.J. Cooksey, M.A.M. Daniels, R. Withnall, R. Indigo, Woad, and Tyrian Purple - Important Vat Dyes from Antiquity to the Present, Endeavour 17 (1993) 191-199.
- [8] P. Friedländer, P. Über den Farbsto des antiken Purpurs aus Murex brandaris, Ber. Dtsch. Chem. Ges. 42 (1909) 765-770.
- [9] P. Friedlaender, Zur Kenntnis des Farbstoffs des antiken Purpurs aus Murex brandaris, Monatshefte für Chemie 28 (1907) 991-996.
- [10] M. Grzybowski, I. Deperasinska, M. Chotkowski, M. Banasiewicz, A. Makarewicz, B. Kozankiewicz, D.T. Gryko, Dipyrrolonaphthyridinediones - structurally unique cross-conjugated dyes, Chemical Communications 52 (2016) 5108-5111.
- [11] R.M. Christie, Why is Indigo Blue?, Biotechnic & Histochemistry 82 (2007) 51-56.
- [12] Otterste.Ja, Photostability and Molecular-Structure, Journal of Chemical Physics 58 (1973) 5716-5725.
- [13] S. Yamazaki, A.L. Sobolewski, W. Domcke, Molecular mechanisms of the photostability of indigo, Physical Chemistry Chemical Physics 13 (2011) 1618-1628.
- [14] I. Izumi, Y. Atushi, K. Takayoshi, Why is Indigo Photostable over Extremely Long Periods?, Chemistry Letters 38 (2009) 1020-1021.
- [15] G.M. Wyman, B.M. Zarnegar, Excited-State Chemistry of Indigoid Dyes .2. Interaction of Thioindigo and Selenoindigo Dyes with Hydroxylic Compounds and Its Implications on Photostability of Indigo, Journal of Physical Chemistry 77 (1973) 1204-1207.
- [16] G. Miehe, P. Susse, V. Kupcik, E. Egert, M. Nieger, G. Kunz, R. Gerke, B. Knieriem, M. Niemeyer, W. Luttko, Theoretical and Spectroscopic Investigations of Indigo Dyes .23. Light-Absorption as Well as Crystal and Molecular-Structure of N,N'-Dimethylindigo - an Example of the Use of Synchrotron Radiation, Angewandte Chemie-International Edition in English 30 (1991) 964-967.
- [17] J. Pina, D. Sarmiento, M. Accoto, P.L. Gentili, L. Vaccaro, A. Galvao, J.S. Seixas de Melo, Excited-State Proton Transfer in Indigo, J. Phys. Chem. B 121 (2017) 2308-2318.
- [18] N.D. Bernardino, S. Brown-Xu, T.L. Gustafson, D.L.A. de Faria, Time-Resolved Spectroscopy of Indigo and of a Maya Blue Simulant, Journal of Physical Chemistry C 120 (2016) 21905-21914.
- [19] G. Grimme, S. Grimme, P.G. Jones, P. Boldt, Am1 and X-Ray Studies of the Structures and Isomerization-Reactions of Indigo Dyes, Chemische Berichte-Recueil 126 (1993) 1015-1021.

- [20] I. Reva, L. Lapinski, M.J. Nowak, Stability of monomeric indigo in the electronic ground state: An experimental matrix isolation infrared and theoretical study, *Dyes Pigments* (2023).
- [21] M. Moreno, J.M. Ortiz-Sanchez, R. Gelabert, J.M. Lluch, A theoretical study of the photochemistry of indigo in its neutral and dianionic (leucoindigo) forms, *Phys Chem Chem Phys* 15 (2013) 20236-20246.
- [22] R. Rondao, J.S. de Melo, M.J. Melo, A.J. Parola, Excited-State Isomerization of Leuco Indigo, *Journal of Physical Chemistry A* 116 (2012) 2826-2832.
- [23] J.S. de Melo, A.P. Moura, M.J. Melo, Photophysical and spectroscopic studies of Indigo derivatives in their keto and leuco forms, *Journal of Physical Chemistry A* 108 (2004) 6975-6981.
- [24] A.S. Chatterley, D.A. Horke, J.R.R. Verlet, On the intrinsic photophysics of indigo: a time-resolved photoelectron spectroscopy study of the indigo carmine dianion, *Phys Chem Chem Phys* 14 (2012) 16155-16161.
- [25] P.P. Roy, J. Shee, E.A. Arsenault, Y. Yoneda, K. Feuling, M. Head-Gordon, G.R. Fleming, Solvent Mediated Excited State Proton Transfer in Indigo Carmine, *J Phys Chem Lett* (2020) 4156-4162.
- [26] M.R. Haggmark, G. Gate, S. Boldissar, J. Berenbeim, A.L. Sobolewski, M.S. de Vries, Evidence for competing proton-transfer and hydrogen-transfer reactions in the S-1 state of indigo, *Chemical Physics* 515 (2018) 535-542.
- [27] T. Cohen, N. Svadlenak, C. Smith, K. Vo, S.-Y. Lee, A. Parejo-Vidal, J.R.A. Kincaid, A.L. Sobolewski, M.F. Rode, M.S. de Vries, Excited-state dynamics of deuterated indigo, *The European Physical Journal D* 77 (2023).
- [28] A.J. Stasyuk, P.J. Cywinski, D.T. Gryko, Excited-state intramolecular proton transfer in 2'-(2'-hydroxyphenyl)imidazo[1,2-pyridines, *J Photoch Photobio C* 28 (2016) 116-137.
- [29] M. Forés, S. Scheiner, Effects of chemical substitution upon excited state proton transfer.: Fluoroderivatives of salicylaldehyde, *Chemical Physics* 246 (1999) 65-74.
- [30] G. Meijer, M.S. de Vries, H.E. Hunziker, H.R. Wendt, Laser Desorption Jet-Cooling of Organic-Molecules: Cooling Characteristics and Detection Sensitivity, *Appl Phys B-Photo* 51 (1990) 395-403.
- [31] F.M. Siouri, S. Boldissar, J.A. Berenbeim, M.S. de Vries, Excited State Dynamics of 6-Thioguanine, *J Phys Chem A* 121 (2017) 5257-5266.
- [32] C. Moller, M.S. Plesset, Note on an approximation treatment for many-electron systems, *Phys Rev* 46 (1934) 618-622.
- [33] C. Hattig, Structure optimizations for excited states with correlated second-order methods: CC2 and ADC(2), *Advances in Quantum Chemistry*, Vol 50 50 (2005) 37-60.
- [34] J. Schirmer, Beyond the Random-Phase Approximation - a New Approximation Scheme for the Polarization Propagator, *Physical Review A* 26 (1982) 2395-2416.
- [35] A.B. Trofimov, J. Schirmer, V.B. Kobychew, A.W. Potts, D.M.P. Holland, L. Karlsson, Photoelectron spectra of the nucleobases cytosine, thymine and adenine, *J Phys B-at Mol Opt* 39 (2006) 305-329.
- [36] D. Tuna, D. Lefrancois, L. Wolanski, S. Gozem, I. Schapiro, T. Andruniów, A. Dreuw, M. Olivucci, Assessment of Approximate Coupled-Cluster and Algebraic-Diagrammatic-Construction Methods for Ground- and Excited-State Reaction Paths and the Conical-Intersection Seam of a Retinal-Chromophore Model, *J Chem Theory Comput* 11 (2015) 5758-5781.
- [37] T.H. Dunning, Gaussian-Basis Sets for Use in Correlated Molecular Calculations .1. The Atoms Boron through Neon and Hydrogen, *Journal of Chemical Physics* 90 (1989) 1007-1023.
- [38] C. Hättig, F. Weigend, CC2 excitation energy calculations on large molecules using the resolution of the identity approximation, *Journal of Chemical Physics* 113 (2000) 5154-5161.
- [39] O. Christiansen, H. Koch, P. Jorgensen, The 2nd-Order Approximate Coupled-Cluster Singles and Doubles Model Cc2, *Chemical Physics Letters* 243 (1995) 409-418.

- [40] TURBOMOLE V7.1 2016, a development of University of Karlsruhe and Forschungszentrum Karlsruhe GmbH, 1989-2007, TURBOMOLE GmbH, since 2007; available from <http://www.turbomole.com>, 2016.
- [41] W.J. Yang, X.B. Chen, Dual fluorescence of excited state intra-molecular proton transfer of HBFO: mechanistic understanding, substituent and solvent effects, *Physical Chemistry Chemical Physics* 16 (2014) 4242-4250.
- [42] M.F. Rode, A.L. Sobolewski, Effect of Chemical Substituents on the Energetical Landscape of a Molecular Photoswitch: An Ab Initio Study, *Journal of Physical Chemistry A* 114 (2010) 11879-11889.
- [43] W.P. Oziminski, J.C. Dobrowolski, σ - and π -electron contributions to the substituent effect: natural population analysis, *Journal of Physical Organic Chemistry* 22 (2009) 769-778.
- [44] J.C. Dobrowolski, P.F.J. Lipinski, G. Karpinska, Substituent Effect in the First Excited Singlet State of Monosubstituted Benzenes, *Journal of Physical Chemistry A* 122 (2018) 4609-4621.
- [45] R.S. Becker, *Theory and interpretation of fluorescence and phosphorescence*, Wiley Interscience 1969.
- [46] M. Rae, F. Perez-Balderas, C. Baleizao, A. Fedorov, J.A.S. Cavaleiro, A.C. Tomé, M.N. Berberan-Santos, Intra- and intermolecular heavy-atom effects on the fluorescence properties of brominated C polyads, *Journal of Physical Chemistry B* 110 (2006) 12809-12814.
- [47] P. Vanhaver, M. Vanderauweraer, L. Viaene, F.C. Deschryver, J.W. Verhoeven, H.J. Vanramesdonk, Enhanced Intersystem Crossing in 3-(1-Pyrenyl)Propylbromide, *Chemical Physics Letters* 198 (1992) 361-366.